ACS APPLIED MATERIALS & INTERFACES

Research Article

www.acsami.org

The Effects of Fluorine-Contained Molecules on Improving the Polymer Solar Cell by Curing the Anomalous S-Shaped *I*–*V* Curve

Chi-Ang Tseng,[†,‡,⊗] Hsieh-Cheng Han,[§,○,⊗] Cheong-Wei Chong,[§,⊥] Ching-Chun Chang,[†] Chi-Feng Lin,[#] Sheng-Bo Wang,[§,▽] Wei-Hsuan Tseng,[∥] Chih-I Wu,[∥] Jiun-Haw Lee,[∥] Shoou-Jinn Chang,[▽] Kuei-Hsien Chen,*[,†,§] and Li-Chyong Chen*[,§]

[†]Institute of Atomic and Molecular Sciences, Academia Sinica, Taipei 10617, Taiwan

[‡]Department of Chemistry, [§]Center for Condensed Matter Sciences, and [∥]Department of Electrical Engineering, Graduate Institute of Photonics and Optoelectronics, National Taiwan University, Taipei 10617, Taiwan

[○]Research Center for Applied Sciences, Academia Sinica, Taipei 11529, Taiwan

[⊥]Department of Physics and [▽]Institute of Microelectronics and Department of Electrical Engineering, National Cheng Kung University, Tainan 701, Taiwan

[#]Department of Electro-Optical Engineering, National United University, Miaoli 36003, Taiwan

Supporting Information

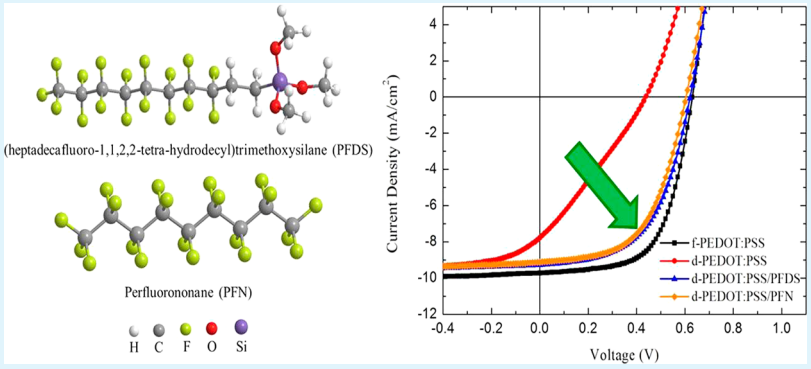

ABSTRACT: In this study, we investigate the effects of fluorinated poly(3,4-ethylene dioxythiophene):poly(styrenesulfonate) buffer layer on the performance of polymer photovoltaic cells. We demonstrate for the first time, the deterioration of the device performance can be effectively mended by modifying the interface between the active layer and buffer layer with heptadecafluoro-1,1,2,2-tetra-hydro-decyl trimethoxysilane (PFDS) and perfluorononane. Device performance shows a substantial enhancement of short-circuit current from 7.90 to 9.39 mA/cm^2 and fill factor from 27% to 53%. The overall device efficiency was improved from 0.98% to 3.12% for PFDS modified device. The mechanism of S-shape curing is also discussed. In addition, the stability of modified devices shows significant improvement than those without modification. The efficiency of the modified devices retains about half (1.88%) of its initial efficiency (4.1%) after 30 d compared to the unmodified ones (0.61%), under air atmosphere.

KEYWORDS: *polymer solar cell, PEDOT:PSS, fluorinated, S-shaped I–V curve, device performance*

INTRODUCTION

Organic solar cells (OSCs) have attracted considerable attention owing to their unique advantages such as low-cost manufacturing and easy processability over large area via screen printing, and roll-to-roll coating technologies.[1,2] At the early stage of the development, solution-processed bulk-heterojunction OSCs showed a power conversion efficiency (PCE) of ∼1%,[3] which was further improved steadily to ∼5% in poly(3-heylthiphene) (P3HT) and [6,6]-phenyl C61-butyric acid methyl ester (PCBM) blend. However, the poor stability is still a major hurdle for their wide range of applications.[4−6] The surface modification and control of interface between the anode or anodic buffer layer and active layer have been reported for improving the device lifetime as well as PCE in solar cells.[7−9] In the past, most studies of the degradation of OSCs have focused upon oxidative damage to the photoactive layer associated with illumination of the device in the presence of molecular oxygen and several light-dependent degradation pathways.[10−12] However, in recent years, numerous reports in the literature have demonstrated that one of the major causes to the device degradation was due to the contacts/interfaces problem.[13−18] Saive et al. showed an increased transport barrier at the PCBM/

Received: January 3, 2015
Accepted: March 13, 2015
Published: March 13, 2015

DOI: 10.1021/acsami.5b00048
ACS Appl. Mater. Interfaces 2015, 7, 6683−6689

cathode interface resulted in a non-ideal cathode interface.[15] Oida et al. reported the degradation was associated with the high series resistance to the injection current at the organic/electrode interface.[17] Meanwhile, several studies showed that the key cause of deteriorated PEDOT:PSS in the device under air exposure is light-independent and, rather, resulted primarily from water absorption by the hygroscopic poly(3,4-ethylenedioxythiophene):poly(4-styrene sulfonate) (PEDOT:PSS) layer.[19,20] On the basis of the electrical characterization, Street et al. also found that the OSC was degraded due to the PEDOT:PSS contacts and the active layer was unaffected even after the ambient exposure.[18] Though the degradation mechanisms can be manifold or even controversial, here we demonstrate a facile method to enhance the performance of OSC, both the $J-V$ characteristics of the as-fabricated device and its stability.

As reported in the literature, a kink has been observed in the $J-V$ curve under illumination instead of the expected diode shape in some cases.[21] This feature, commonly called as S-shape, leads to reduced solar cell parameters such as fill factor and Jsc and/or Voc. It had been reported that S-shaped $J-V$ curve results from the devices fabricated from the air-exposed PEDOT:PSS.

Some possible mechanisms of S-shape curve formation have been proposed. However till date no such literature exists to answer how to solve this problem or further discuss the different proposed mechanism. Interface engineering provides some opportunity for changing the surface wettability[22] or tuning the dipole direction[23] and the electrical property of the modified layer,[24] thus enhancing the corresponding device efficiency.

In this letter, we first investigate the effects of moisture damage of PEDOT:PSS layers on solar cell device performance. It was found that the S-shape can be controlled by tuning the air exposure time. A simple method to mend the S-shape characteristic by modifying the surface of PEDOT:PSS with (heptadecafluoro-1,1,2,2-tetrahydrodecyl)trimethoxysilane ($C_{13}H_{13}F_{17}O_3Si$, PFDS) and perfluorononane (PFN) is demonstrated to be effective for enhancing the device efficiency and stability. Finally, we also discuss the possible mechanism behind the curing of S-shaped curve.

EXPERIMENTAL SECTION

The polymer solar cells in this work have two different structures. Standard device structure is based on glass/ITO/PEDOT:PSS/P3HT:PCBM/BCP/Ag, and modified device is based on glass/ITO/PEDOT:PSS/PFAS or PFN/P3HT:PCBM/BCP/Ag as shown in Figure 1. BCP is 2,9-dimethyl-4,7-diphenyl-1,10-phenanthroline, which acts as the hole-blocking layer, and ITO is indium tin oxide.

The ITO-coated glass (15 $\Omega\cdot cm^{-2}$) was cleaned using standard procedure (cleaning under ultrasonic bath in detergent solution followed by acetone and isopropyl alcohol). A buffer layer of PEDOT:PSS (CLEVIOS P VP AI 4083) was obtained by spin coating an aqueous solution onto ITO-coated glass substrates. It was then annealed at 150 °C for 20 min under nitrogen ambient. The optimized conditions of the PEDOT:PSS were similar to those in Chang et al.[25]

The impact of the degraded PEDOT:PSS layers on device performance was investigated by monitoring the annealed PEDOT:PSS-coated ITO samples that were stored in five different humidity environments for 24 h. For the humidity control, various drying agents were placed together with the samples. Six samples were prepared and labeled as (1) to (6) that represent different humidity conditions. The used drying agents were (1) $MgSO_4$ and Na metal (each with more than 50 g inside desiccator with N_2 ambient), (2) inside glovebox with N_2 ambient (humidity below 10 ppb), (3) $MgSO_4$ only (50 g inside desiccator with N_2 ambient), (4) in desiccator box for 1 h and then transfer into N_2 ambient (inside glovebox) and (5) in air. Because of the different hygroscopicity of these drying agents, hereafter, the samples are designated according to the different humidity conditions, following the trend where humidity of sample (1) < (2) < (3) < (4) < (5). Also note that fresh PEDOT:PSS device (designated as sample 6) refers to the one subjected to immediate casting of the active layer right after annealing of PEDOT:PSS. The modifiers, PFDS and PFN, were dissolved in chlorobenzene (CB) for spin-coating. The PFDS- or PFN-modified PEDOT−PSS was then annealed at 150 °C for 20 s. After that, solutions containing P3HT and PCBM of 1:0.6 weight ratio dissolved in CB were cast on top of the PEDOT:PSS to form thin films that were then annealed again at 150 °C for 20 min. Contact angle measurements were done to confirm the presence of PFDS and PFN after the active-layer coating. The samples were then transferred to a vacuum chamber where BCP and Al layers of thicknesses 5 and 100 nm, respectively, were deposited by an INFICON T054 thermal evaporator.

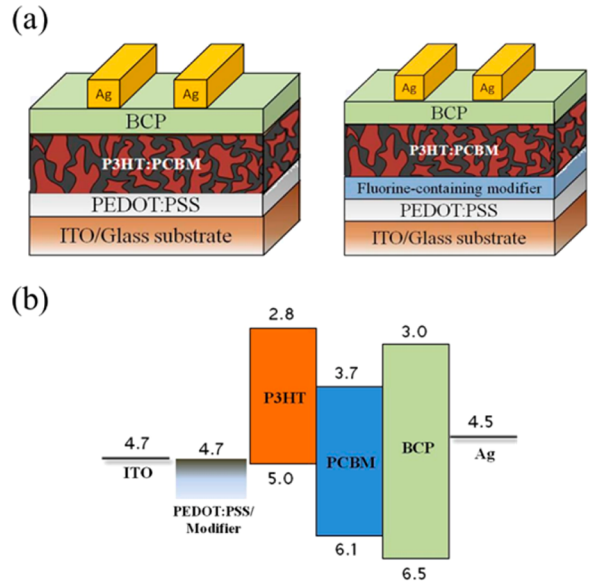

Figure 1. Schematics of the photovoltaic device structure consisting of the following: (a) ITO/PEDOT:PSS/P3HT:PCBM/BCP/Ag (left). ITO/PEDOT:PSS/PFDS or PFN/P3HT:PCBM/BCP/Ag (right). (b) Band alignment of photovoltaic device in this work.

The current density versus voltage ($J-V$) characteristics of the devices were measured with an $I-V$ source meter (Keithley 2400) under the dark condition and under the illumination of an AM 1.5G, 1-sun solar simulator (Newport's Sol2A Class ABA Solar Simulators), which was calibrated through a Si reference cell. Conductivity measurements were done in air using four-point-probe technique. The Fourier transform infrared (FT-IR) measurements were performed at a Nicolet 6700 FT-IR spectrometer, using continuum FT-IR microscope attachment (scan 512 times) and mercury cadmium telluride (MCT) detector. X-ray photoelectron spectroscopy (XPS) of PEDOT:PSS deposited on ITO/glass substrate was done using a VG Scientific ESCALAB 250 spectrometer with a base pressure of 5×10^{-10} mbar (UHV) and monochromatized Al radiation 15 kV.

RESULTS AND DISCUSSION

Effect of Moisture Condition. The effects of the moisture were assessed based on device performance. Figure 2a shows the $J-V$ characteristics for all devices under different humidity conditions. Device with fresh PEDOT:PSS had an efficiency of 4.11% and a fill factor of 0.63 (Table 1) with a quite ideal $J-V$ curve. However, device efficiency gradually decreases with

DOI: 10.1021/acsami.5b00048
ACS Appl. Mater. Interfaces 2015, 7, 6683−6689

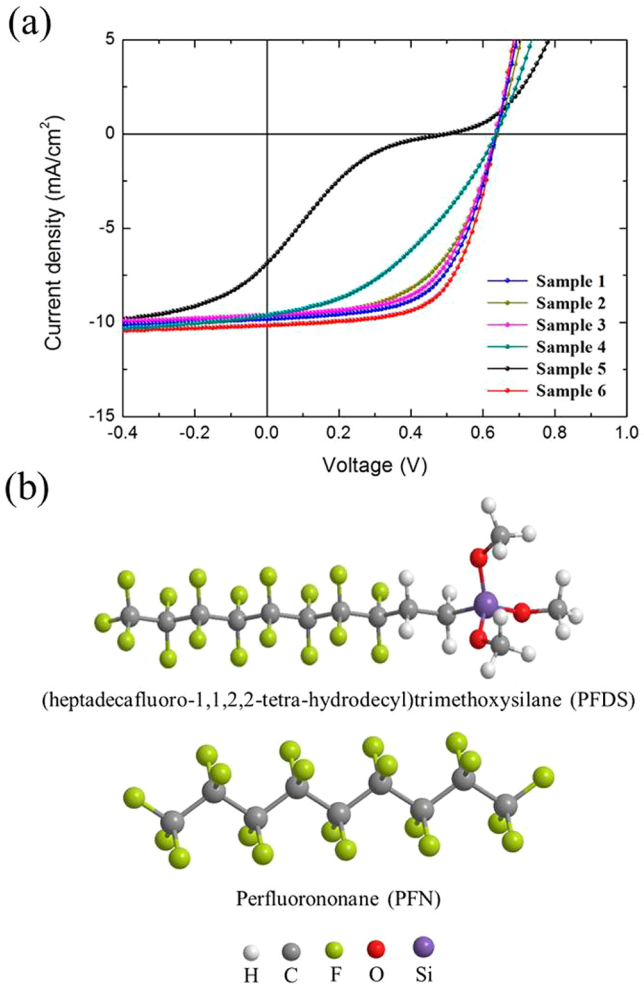

Figure 2. (a) The $J-V$ characteristics and parameters for all devices under different humidity conditions. (b) Chemical structure of PFDS and PFN used in this work.

increase in the humidity. Also note that all parameters of the device with PEDOT:PSS in air for 3 d show larger reduction and also exhibit anomalous S-shaped curve with an efficiency of 0.47% and a fill factor of only 0.15. From these results, we know that the S-shape phenomenon of $J-V$ curves obviously plays a significant role in device performance. Similar phenomenon has been observed in the literature.[26−28] Reports have shown that such phenomenon was due to (1) the presence of interfacial dipole where the direction is opposite to the built-in potential,[29] (2) the reduction of hole surface recombination velocity at the anodic interface,[30] and (3) formation of hole injection barrier between the active polymer layer and the hole transporting layer.[31] Nonetheless, until now, there exists no demonstration for curing the S-shape. Furthermore, by trying to solve this problem, we simultaneously have a better understanding about the dominant underlying mechanism causing the formation of S-shaped $J-V$ curve.

To cure the S-shaped $J-V$ curve caused by water moisture deterioration, surface modification on hydrophilic PEDOT:PSS layers was performed with two kinds of fluorine-containing materials, namely, PFDS and PFN, which are hydrophobic linear structures with high electron-affinity fluorine atoms as shown in Figure 2b. PFDS has a silane functional group, so we expect that the whole molecule might stand on surface and dipoles will be formed at the interfaces, which will benefit the charge-transporting property between PEDOT:PSS layer and active materials. In contrast, PFN molecule will have better penetration ability into PEDOT:PSS layer due to the absence of silane group.

Effect of PFDS and PFN Modification. To investigate the curing of the degraded PEDOT:PSS, four kinds of samples were fabricated. They were (A) fresh PEDOT:PSS, (B) degraded PEDOT:PSS, (C) degraded PEDOT:PSS with 0.1% PFDS modification, and (D) degraded PEDOT:PSS with 0.1% PFN modification. Degraded samples are those that experienced the degradation process in which they were exposed to air ambient for 24 h. Comparative $J-V$ measurements were performed to evaluate the resultant device performance, with and without the modifiers, after the degradation process. Figure 3 shows the $J-V$ characteristics of samples A-D. Device B with

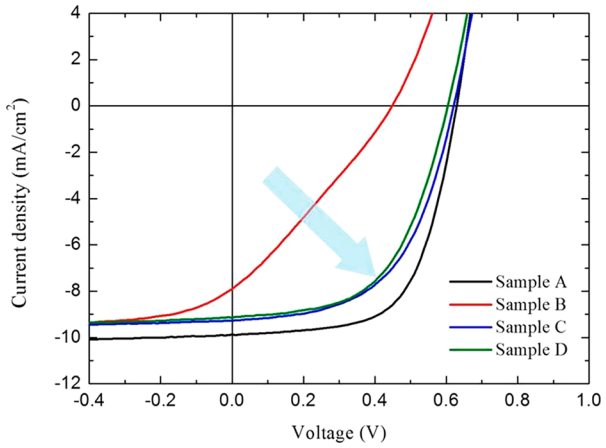

Figure 3. $J-V$ characteristics and device parameters for samples A to D.

degraded PEDOT:PSS shows S-shape characteristics and the efficiency dramatically decreases about one-quarter, corresponding to the Voc from 0.63 to 0.45 V and Jsc from 9.79 to 7.90 mA/cm^2 (Table 2). However, the modified devices C and D show ~3 times enhancement compared to the unmodified device B, corresponding to improved efficiency from 0.98% to 3.12% and 3.04%, respectively. Remarkably, this

Table 1. Device Performance for Samples 1 to 6

conditions	V_{oc} [V]	J_{sc} [mA cm^{-2}]	FF [%]	PCE [%]	R_{sh} (Ωcm^2)	R_s [Ωcm^2]
sample 1	0.63 ± 0.01	9.76 + 0.42	60	3.72 ± 0.16	948.9	6.2
sample 2	0.65 ± 0.01	9.55 + 0.38	57	3.52 ± 0.12	772.4	6.7
sample 3	0.64 ± 0.01	9.38 + 0.28	56	3.36 ± 0.18	856.0	7.1
sample 4	0.64 + 0.00	10.02 + 0.28	41	2.61 + 0.28	388.6	9.5
sample 5	0.49 + 0.02	6.47 + 0.62	15	0.47 + 0.09	50.9	17.5
sample 6	0.64 + 0.01	10.22 + 0.29	63	4.11 + 0.15	1264.0	6.0

DOI: 10.1021/acsami.5b00048
ACS Appl. Mater. Interfaces 2015, 7, 6683−6689

Table 2. Devices Performance for Samples A to D

conditions	V_{oc} [V]	J_{sc} [mA cm^{-2}]	FF [%]	PCE [%]	R_{sh} [Ω cm^2]	Rs [Ω cm^2]
sample A	0.63 ± 0.01	9.41 ± 0.42	62.73	3.74 ± 0.13	744.85	5.5
sample B	0.49 + 0.03	8.36 + 0.33	33.38	1.37 + 0.28	68.50	13.01
sample C	0.62 + 0.00	9.39 + 0.14	53.40	3.12 + 0.07	314.71	7.59
sample D	0.61 ± 0.01	9.12 ± 0.17	55.08	3.04 ± 0.08	383.32	7.20

is the first demonstration that an S-shaped $J-V$ curve can be cured near to its normal state. Nevertheless, to study whether the degradation could also be recovered by merely heating the degraded sample (due to dehydration), further heating at 180 °C for 3 min was done for the unmodified degraded sample. As shown in Supporting Information, Figure S1, clear S-shaped $J-V$ is still observed, indicating mere heating is not effective to recover the device performance. We should notice here that the effect of PFDS and PFN is almost comparable, although a different mechanism contributes for S-shape curing, which will be discussed later.

XPS and water droplet contact angle measurements were used to confirm the presence of the modified materials. F(1s) core spectra of samples C and D are shown in Figure 4a. The

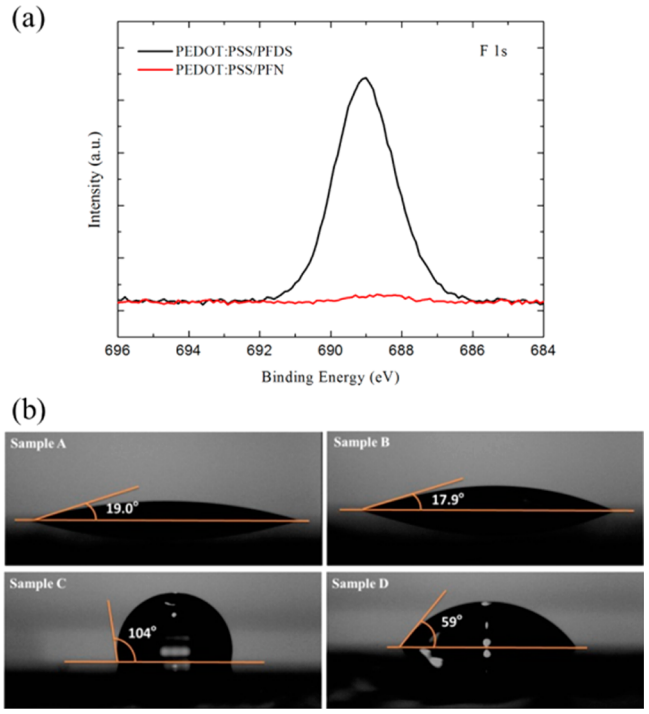

Figure 4. (a) F(1s) core spectra of samples C and D. (b) Images of a water droplet on samples B–D.

peaks at ~689 eV originate from the C–F bond. It is observed that sample C shows higher intensity than sample D, due to presence or absence of silane anchoring group in these two materials. Figure 4b shows the contact angle images of samples A–D. It is well-known that the pristine PEDOT:PSS is superhydrophilic, corresponding to a contact angle of 19° (sample A), and the degraded PEDOT:PSS (sample B) shows comparable contact angle value (17.9°). However, PFDS (sample C) and PFN (sample D) modified PEDOT:PSS show more hydrophobic property compared to pristine PEDOT:PSS with the contact angles of 104° and 59°, respectively. Note that the higher concentrations of PFDS and PFN solutions, the thinner of the following active layer forms. Because of the lower surface energy, the active layer will form very poor thin film when PFDS solution with concentration higher than 0.1% was used. However, smaller effect was observed in the case of PFN solution when the concentration was higher than 0.1%.

Figure 5a shows the secondary electron cutoffs from ultraviolet photoelectron spectra (UPS) obtained from samples

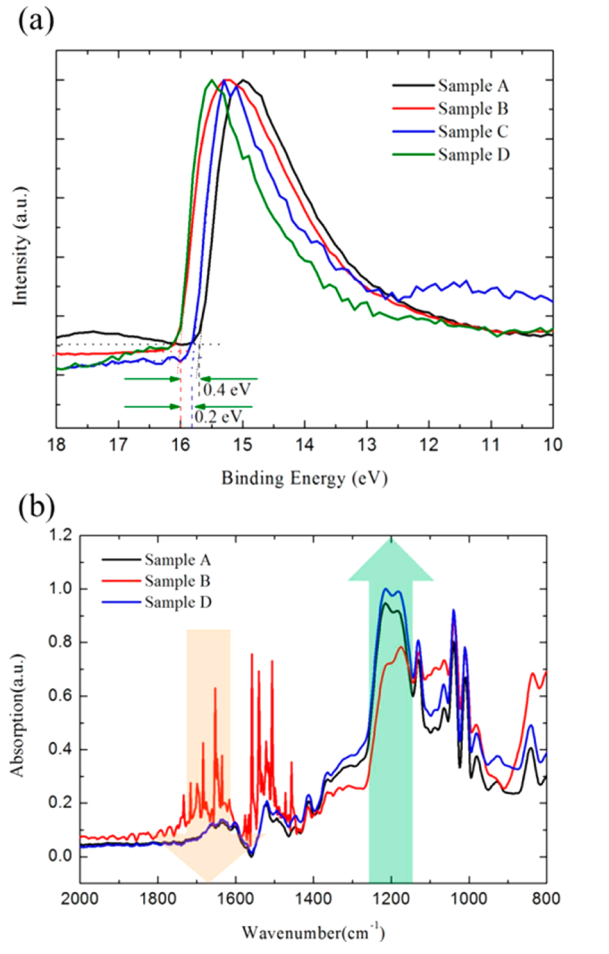

Figure 5. (a) The secondary electron cutoffs from UPS obtained from samples A to D. (b) The FTIR measurement of samples A, B, and D.

A–D. It shows that the onset of the secondary electron cutoffs of sample B shifted to higher binding energy by 0.4 eV relative to that of sample A, indicating the presence of an interfacial dipole decreases the vacuum level of samples B, leading to a barrier for the charge transport.[32] In contrast, the onset of sample C shifted to lower binding energy by 0.2 eV relative to that of sample B, implying that the dipole at the PEDOT:PSS/active layer interface pointed to PFDS-modified PEDOT:PSS, leading to an increase in built-in potential. However, the

DOI: 10.1021/acsami.5b00048
ACS Appl. Mater. Interfaces 2015, 7, 6683–6689

secondary electron cutoffs of sample D did not show an obvious difference when compared with sample B.

To further understand the possible mechanism of PFN curing, we proceeded with other measurements. As mentioned above, we expect PFN has better penetration ability into PEDOT:PSS layer. Thus, FTIR measurement is performed. The FTIR spectra of samples A, B,and D are shown in Figure 5b. The peaks appearing at 1644, 1180, 1127, 1037, and 1008 cm^{-1} are contributed from the stretching vibration of C−C aromatic skeleton, SO_3^- group symmetric vibration, in-plane skeleton vibration of phenyl ring, SO_3^- group antisymmetric vibration, and in-plane bonding vibration of phenyl ring, respectively.[33] The FTIR results of poly(styrene sulfonic acid) (PSSA) hydrogel in different salt solutions have been discussed.[34] They found that the intensity of the 1644 cm^{-1} peak in deionized water is much higher than the 1000−1200 cm^{-1} ones, implying that the 1644 cm^{-1} peak has been significantly interfered by the presence of water. On the contrary, in KF solutions, the 1000−1200 cm^{-1} peak has become much stronger than that at 1644 cm^{-1} due to the dehydration of PSSA hydrogel and the presence of fluorine ion near hydrated SO_3^-. We also observed that the 1644 cm^{-1} peak of sample B is much higher than the 1000−1200 cm^{-1} ones, indicating that the SO_3^- group was blocked by the presence of water. However, the 1000−1200 cm^{-1} peak of sample D became much stronger than that at 1644 cm^{-1}. It may imply that PFN molecules partially penetrate into the PEDOT:PSS film to dehydrate the water-blocked SO_3^- group.

The penetration of PFN can be clearly observed by XPS depth profile measurement. Figure 6 shows the XPS depth profile with samples C and D. The results show that the PFDS molecule located mainly at the surface of PEDOT:PSS. However, the modification with PFN molecule always shows the F 1s signal within the depth of 5 nm. We suggested that the diffusion of PFN molecule might happen when the active layer was annealed at 150 °C for 20 min. This result can support the FTIR results about the dehydration of water-blocked SO_3^- group and to make evident our early expectation that the PFN molecule without silane group may have better penetration ability into thin film.

To investigate how the PFN penetration affects the device characteristics, the conductivities of samples A to D were measured by four-point probe technique. Sample A shows the best conductivity of 5.17×10^{-2} S cm^{-1} with the least air-exposed time, but the conductivity of sample B was greatly reduced to 3.27×10^{-5} S cm^{-1}. However, once modifying PEDOT:PSS with PFDS and PFN (samples C and D), the conductivity can be recovered by almost 2 orders of magnitude larger to 1.34×10^{-3} S cm^{-1} and 1.37×10^{-3} S cm^{-1}, respectively. The enhancement of conductivity after PFDS (sample C) and PFN (sample D) modification is attributed to two different mechanisms, the preferred dipole formation at the interface for PFDS and the hopping center recovery of SO_3^- group for PFN, which we mentioned above.

Stability of PFN-Modified Device. Finally, to demonstrate the function of PFN material for preventing PEDOT:PSS from moisture damage, we make the devices with fresh PEDOT:PSS (sample A) and PFN-modified PEDOT:PSS (sample D) exposed to atmospheric air for different times. The illuminated $J-V$ characteristics of the OCSs exposed to atmospheric air for different times is shown in Figure 7a, and Figure 7b shows the influence of the air-exposure duration time of the devices on all parameters of PCE, Jsc, Voc, and FF. The

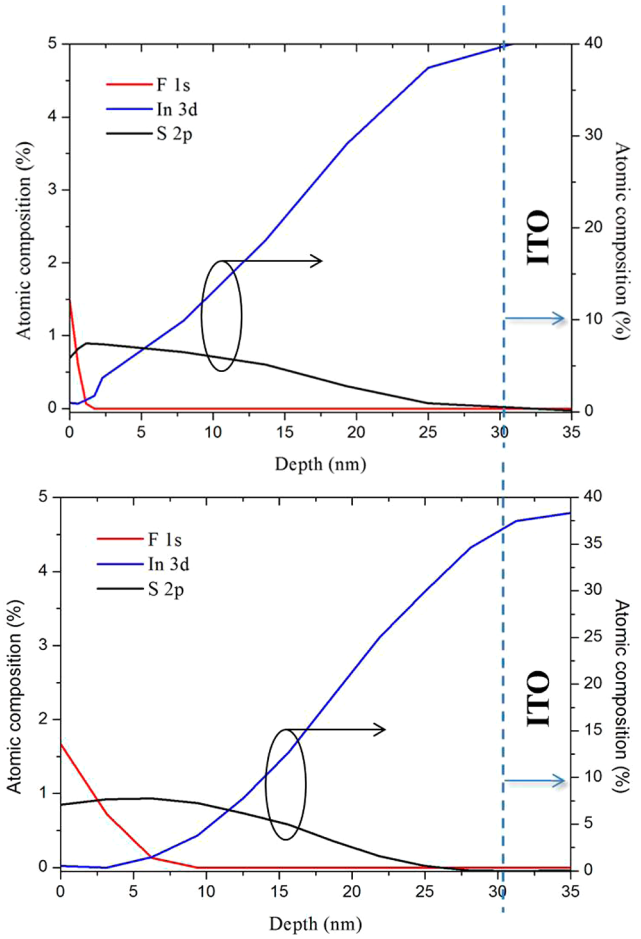

Figure 6. XPS depth profile of sample C (upper) and D (lower).

performance of the device with PFN-modified PEDOT:PSS (Figure 7c) is better than that with pristine PEDOT:PSS for the same time intervals of air exposures. When the devices are exposed to air for 60 d, a PCE of 1.88% is recorded for the device with PFN-modified PEDOT:PSS, but the PCE of the device with pristine PEDOT:PSS is 0.61%. Commercial organic solar panels might need the protecting coating barrier against the absorption of air. Our result shows that the formation of hydrophobic layer on the PEDOT:PSS surface may protect PEDOT:PSS from water deterioration, which may minimize the unavoidable degradation during the fabrication process and is propitious to improve the stability of OSC eventually.

CONCLUSIONS

In this work, we investigated the effects of moisture deterioration of PEDOT:PSS buffer layer on the performance of polymer photovoltaic cells. We demonstrated, for the first time, the device with damaged PEDOT:PSS can be effectively recovered by modifying the interface with PFDS and PFN materials. The overall device efficiency shows obvious enhancement to 3.12% for PFDS and 3.04% for PFN, compared with 0.98% for degraded PEDOT:PSS device. We also proposed that the mechanism of S-shape curing is attributed to the beneficial dipole formation for PFDS modification, which improves the transport ability over the interface, and the dehydration of water-blocked SO_3^- group due to the good penetration ability of PFN, which recovers the conductivity of the buffer layer. The device stability is also enhanced by using PFN-modified

DOI: 10.1021/acsami.5b00048
ACS Appl. Mater. Interfaces 2015, 7, 6683−6689

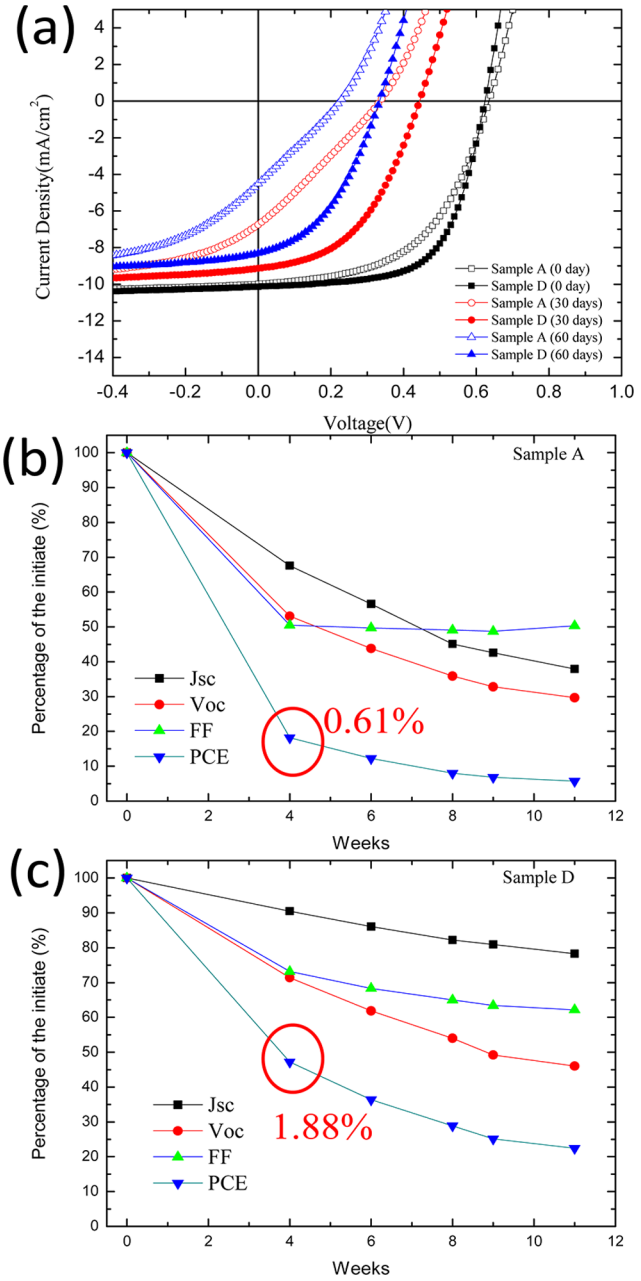

Figure 7. (a). The *J*–*V* characteristics and (b) device stability test for sample A and (c) sample D.

PEDOT:PSS with PCE of 1.88% compared to control device of 0.61% after 60 d. This stability enhancement can be attributed to the protection of hydrophobic layer on the PEDOT:PSS surface from water absorption.

■ ASSOCIATED CONTENT

Supporting Information

Illustration of the comparison between the effect of heating and PFDS modification on the device performance, monitored by the *J*–*V* measurement. This material is available free of charge via the Internet at http://pubs.acs.org.

■ AUTHOR INFORMATION

Corresponding Authors

*Phone: +886-2-33665200. E-mail: chenlc@ntu.edu.tw. (L.-C.C.)

*E-mail: chenkh@pub.iams.sinica.tw. Phone: +886-2-23668232. (K.-H.C.)

Author Contributions

⊗These authors contributed equally. The manuscript was written through contributions of all authors. All authors have given approval to the final version of the manuscript.

Funding

This research was financially supported by the Ministry of Education, National Science Council, Academia Sinica (Taiwan), and Asian Office of Aerospace Research and Development under AFOSR.

Notes

The authors declare no competing financial interest.

■ ACKNOWLEDGMENTS

Technical support was provided by the Core Facilities for Nano Science and Technology, Academia Sinica, and National Taiwan University.

■ REFERENCES

(1) Krebs, F. C. Fabrication and Processing of Polymer Solar Cells: A Review of Printing and Coating Techniques. *Sol. Energy Mater. Sol. Cells* **2009**, *93*, 394–412.

(2) Krebs, F. C.; Tromholt, T.; Jørgensen, M. Upscaling of Polymer Solar Cell Fabrication Using Full Roll-To-Roll Processing. *Nanoscale* **2010**, *2*, 873–86.

(3) Yu, G.; Gao, J.; Hummelen, J. C.; Wudl, F.; Heeger, A. J. Polymer Photovoltaic Cells: Enhanced Efficiencies via a Network of Internal Donor-Acceptor Heterojunctions. *Science* **1995**, *270*, 1789–1791.

(4) Wu, H. R.; Song, Q. L.; Wang, M. L.; Li, F. Y.; Yang, H.; Wu, Y.; Huang, C. H.; Ding, X. M.; Hou, X. Y. Stable Small-Molecule Organic Solar Cells with 1,3,5-tris(2-*N*-phenylbenzimidazolyl) Benzene as an Organic Buffer. *Thin Solid Films* **2007**, *515*, 8050–8053.

(5) Lo, M. F.; Ng, T. W.; Lai, S. L.; Wong, F. L.; Fung, M. K.; Lee, S. T.; Lee, C. S. Operation Stability Enhancement in Organic Photovoltaic Device by a Metal Doped Organic Exciton Blocking Layer. *Appl. Phys. Lett.* **2010**, *97*, 143304.

(6) Moliton, A.; Nunzi, J. M. How to Model the Behaviour of Organic Photovoltaic Cells. *Polym. Int.* **2006**, *55*, 583–600.

(7) Ryu, M. S.; Jang, J. Effect of Solution Processed Graphene Oxide/Nickel Oxide Bi-Layer on Cell Performance of Bulk-Heterojunction Organic Photovoltaic. *Sol. Energy Mater. Sol. Cells* **2011**, *95*, 2893–2896.

(8) Lo, M. F.; Ng, T. W.; Lai, S. L.; Fung, M. K.; Lee, S. T.; Lee, C. S. Stability Enhancement in Organic Photovoltaic Device by Using Polymerized Fluorocarbon Anode Buffer Layer. *Appl. Phys. Lett.* **2011**, *99*, 033302.

(9) Dong, Q.; Zhou, Y.; Pei, J.; Liu, Z.; Li, Y.; Yao, S.; Zhang, J.; Tian, W. All-Spin-Coating Vacuum-Free Processed Semi-transparent Inverted Polymer Solar Cells with PEDOT:PSS Anode and PAH-D Interfacial Layer. *Org. Electron.* **2010**, *11* (7), 1327–1331.

(10) Kroon, J. M.; Wienk, M. M.; Verhees, W. J. H.; Hummelen, J. C. Accurate Efficiency Determination and Stability Studies of Conjugated Polymer/Fullerene Solar Cells. *Thin Solid Films* **2002**, *223–228*, 403–404.

(11) Neugebauer, H.; Brabec, C.; Hummelen, J. C.; Sariciftci, N. S. Stability and Photodegradation Mechanisms of Conjugated Polymer/Fullerene Plastic Solar Cells. *Sol. Energy Mater. Sol. Cells* **2000**, *61*, 35–42.

(12) Jeranko, T.; Tributsch, H.; Sariciftci, N. S.; Hummelen, J. C. Patterns of Efficiency and Degradation of Composite Polymer Solar Cells. *Sol. Energy Mater. Sol. Cells* **2004**, *83*, 247–262.

(13) delPozo, G.; Romero, B.; Arredondo, B. Evolution with Annealing of Solar Cell Parameters Modeling the S-shape of The Current-Voltage Characteristic. *Sol. Energy Mater. Sol. Cells* **2010**, *104*, 81–86.

DOI: 10.1021/acsami.5b00048
ACS Appl. Mater. Interfaces 2015, 7, 6683–6689

(14) Wagner, J.; Gruber, M.; Wilke, A.; Tanaka, Y.; Topczak, K.; Steindamm, A.; Hörmann, U.; Opitz, A.; Nakayama, Y.; Ishii, H.; Pflaum, J.; Koch, N.; Brütting, W. Identification of Different Origins for S-shaped Current Voltage Characteristics in Planar Heterojunction Organic Solar Cells. *J. Appl. Phys.* **2012**, *111*, 054509.
(15) Saive, R.; Mueller, C.; Schinke, J.; Lovrincic, R.; Kowalsky, W. Understanding S-shaped Current-Voltage Characteristics of Organic Solar Cells: Direct Measurement of Potential Distributions by Scanning Kelvin Probe. *Appl. Phys. Lett.* **2013**, *103*, 243303.
(16) Yang, W.; Yao, Y.; Wu, C. Q. Mechanisms of Device Degradation in Organic Solar Cells: Influence of Charge Injection at the Metal/Organic Contacts. *Org. Electron.* **2013**, *14*, 1992−2000.
(17) Oida, T.; Harafuji, K. Attempt to Suppress S-Shaped Kink in Current−Voltage Characteristics in Organic Solar Cells. *Jpn. J. Appl. Phys.* **2013**, *52*, 011601.
(18) Street, R. A.; Khlyabich, P. P.; Thompson, B. C. Electrical Characterization of Organic Solar Cell Contact Degradation Resulting from Ambient Exposure. *Org. Electron.* **2013**, *14*, 2932−2939.
(19) Kawano, K.; Pacios, R.; Poplavskyy, D.; Nelson, J.; Bradley, D.; Durrant, J. R. Degradation of Organic Solar Cells Due to Air Exposure. *Sol. Energy Mater. Sol. Cells* **2006**, *90*, 3520−3530.
(20) Gevorgyan, S. A.; Jørgensen, M.; Krebs, F. C.; Sylvester-Hvid, K. O. A Compact Multi-Chamber Setup for Degradation and Lifetime Studies of Organic Solar Cells. *Sol. Energy Mater. Sol. Cells* **2011**, *95*, 1389−1397.
(21) Sharma, A.; Watkins, S. E.; Lewis, D. A.; Andersson, G. Effect of Indium and Tin Contamination on the Efficiency and Electronic Properties of Organic Bulk Hetero-Junction Solar Cells. *Sol. Energy Mater. Sol. Cells* **2011**, *95*, 3251−3255.
(22) Han, H. C.; Tseng, C. A.; Du, C. Y.; Ganguly, A.; Chong, C. W.; Wang, S. B.; Lin, C. F.; Su, C. C.; Lee, J. H.; Chen, K. H.; Chen, L. C. Enhancing efficiency with Fluorinated Interlayers in Small Molecule Organic Solar Cells. *J. Mater. Chem.* **2012**, *22*, 22899−22905.
(23) Beaumont, N.; Hancox, I.; Sullivan, P.; Hatton, R. A.; Jones, T. S. Increased Efficiency in Small Molecule Organic Photovoltaic Cells through Electrode Modification with Self-Assembled Monolayers. *Energy Environ. Sci.* **2011**, *4*, 1708−1711.
(24) Sun, K.; Xia, Y.; Ouyang, J. Improvement in the Photovoltaic Efficiency of Polymer Solar Cells by Treating the Poly(3,4-ethylenedioxythiophene):Poly(styrenesulfonate) Buffer Layer with Co-solvents of Hydrophilic Organic Solvents and Hydrophobic 1,2-Dichlorobenzene. *Sol. Energy Mater. Sol. Cells* **2012**, *97*, 89−96.
(25) Chang, C. C.; Lin, C. F.; Chiou, J. M.; Ho, T. H.; Tai, Y.; Lee, J. H.; Chen, Y. F.; Wang, J. K.; Chen, L. C.; Chen, K. H. Effects of Cathode Buffer Layers on the Efficiency of Bulk- Heterojunction Solar Cells. *Appl. Phys. Lett.* **2010**, *96*, 263506.
(26) Uhrich, C.; Schueppel, R.; Petrich, A.; Pfeiffer, M.; Leo, K.; Brier, E.; Kilickiran, P.; Baeuerle, P. Organic Thin-Film Photovoltaic Cells Based on Oligothiophenes with Reduced Bandgap. *Adv. Funct. Mater.* **2007**, *17*, 2991−2999.
(27) Krebs, F. C.; Norrman, K. Analysis of the Failure Mechanism for a Stable Organic Photovoltaic During 10 000 h of Testing. *Prog. Photovoltaics* **2007**, *15*, 697−712.
(28) Wang, J. C.; Ren, X. C.; Shi, S. Q.; Leung, C. W.; Chan, P. K. L. Charge Accumulation Induced S-shape *J*−*V* Curves in Bilayer Heterojunction Organic Solar Cells. *Org. Electron.* **2011**, *12*, 880−885.
(29) Kumar, A.; Sista, S.; Yang, Y. Dipole Induced Anomalous S-shape *I-V* Curves in Polymer Solar Cells. *J. Appl. Phys.* **2009**, *105*, 094512.
(30) Wagenpfahl, A.; Rauh, D.; Binder, M.; Deibel, C.; Dyakonov, V. S-shaped Current-Voltage Characteristics of Organic Solar Devices. *Phys. Rev. B* **2010**, *82*, 115306.
(31) Zhang, M.; Wang, H.; Tang, C. W. Hole-Transport Limited S-shaped *I-V* Curves in Planar Heterojunction Organic Photovoltaic Cells. *Appl. Phys. Lett.* **2011**, *99*, 213506.
(32) Ishii, H.; Sugiyama, K.; Ito, E.; Seki, K. Energy Level Alignment and Interfacial Electronic Structures at Organic/Metal and Organic/Organic Interfaces. *Adv. Mater.* **1999**, *11*, 605.
(33) Jamróz, D.; Maréchal, Y. Hydration of Sulfonated Polyimide Membranes. II. Water Uptake and Hydration Mechanisms of Protonated Homopolymer and Block Copolymers. *J. Phys. Chem. B* **2005**, *109*, 19664−75.
(34) Xu, L.; Li, X.; Zhai, M.; Huang, L.; Peng, J.; Li, J.; Wei, G. Ion-Specific Swelling of Poly(styrene sulfonic acid) Hydrogel. *J. Phys. Chem. B* **2007**, *111*, 3391−3397.

DOI: 10.1021/acsami.5b00048
ACS Appl. Mater. Interfaces 2015, 7, 6683−6689